Lehrstuhl für Bildverarbeitung
Institute of Imaging & Computer Vision

Vessel Segmentation and Analysis in Laboratory Skin Transplant Micro-angiograms

Alexandru Condurache and Til Aach and Stephan Grzybowski and Hans-Günter Machens

in: 18th IEEE Symposium on Computer-Based Medicine (CBMS 2005). See also BIBTEX entry below.

BIBTEX:

```
@inproceedings{CON05d,
author = {Alexandru Condurache and Til Aach and Stephan Grzybowski and
                          Hans-G\"unter Machens},
title = {Vessel Segmentation and Analysis in Laboratory Skin Transplant
                          Micro-angiograms},
booktitle = {18th IEEE Symposium on Computer-Based Medicine (CBMS 2005)},
editor = {A.\ Tsymbal and P.\ Cunningham},
publisher = {IEEE},
address = {Dublin},
month = {June 23--24},
year = {2005},
pages = {21--26}}
```


document created on: December 20, 2006
created from file: cbms05coverpage.tex
cover page automatically created with CoverPage.sty
(available at your favourite CTAN mirror)

RWTH AACHEN
RHEINISCH-WESTFÄLISCHE TECHNISCHE HOCHSCHULE AACHEN

Vessel Segmentation and Analysis in Laboratory Skin Transplant Micro-angiograms

Alexandru Condurache, Til Aach*
Institute for Signal Processing
University of Lübeck
D-23538 Lübeck, Germany
condura@isip.uni-luebeck.de

Stephan Grzybowski, Hans-Günter Machens
Dept. of Plastic and Hand Surgery, Burn Center
University Hospital of Schleswig-Holstein
D-23538 Lübeck, Germany
machens@uni-luebeck.de

Abstract

The success of skin transplantations depends on the adequate revascularization of the transplanted dermal matrix. To induce vessel growth or angiogenesis, pharmacological substances may be applied to the dermal matrix. The effectiveness of different such substances has been evaluated in laboratory experiments. For this purpose, the surface and length of newly grown vessels have to be measured in micro-angiograms (x-ray images of the blood vessels recorded after the injection of a radiopaque substance) of tissue transplanted on the back of laboratory animals. To this end we describe in this contribution a vessel analysis environment central to which is a semi-automatic vessel segmentation tool for surface quantification in fasciocutaneous skin transplant micro-angiograms.

1. Introduction

In the transplanted skin tissue, angiogenesis may be stimulated by administering certain drugs [9]. To evaluate the success of such a treatment laboratory experiments have been conducted. Disk-shaped dermal matrices (diameter: 15mm) were transplanted on the backs of small laboratory animals. For vessel imaging, blood is withdrawn via the left carotid artery, and replaced by a contrast medium. The transplant sample is then harvested and imaged using an X-ray mammography system. A micro-angiogram thus obtained shows the vessels, potentially down to a size of about $20\mu m$ [9], and is depicted in Fig. 1a. On the thus acquired micro-angiograms we seek to quantify the angiogenesis in the target tissue, e.g. by measures such as the percentage of area covered by the blood vessels in the target sample or the vessel length [9]. To this end, the vessels need to be identified in the imaged transplant. Therefore in this contribution we present a method for segmenting the vessels in skin transplant micro-angiograms for angiogenesis analysis tasks.

Vessel segmentation algorithms typically follow a two step approach [12]: (i) vessel enhancement/feature extraction and (ii) segmentation. The feature extraction purpose is to achieve a separable representation of vessel and background pixel classes. In many cases this representation is actually a vessel map (i.e. each pixel is described by a 1D feature) where vessel-like structures are enhanced using e.g. matched filters [10], the eigenvalues of the Hessian matrix at different scales [7] or other methods [5]. In the article by Staal [15] however, a multidimensional pixel representation is used. Several pixel features are proposed and the best pixel feature set is found by sequential feature selection. The vessels are then segmented in a supervised manner using the k-nearest neighbors classifier. Vessel segmentation can also be done in an unsupervised manner by e.g. region

*Til Aach is now with Inst. of Imag. and Comp. Vis., RWTH Aachen University, D-52056 Aachen, Germany

growing [14], tracking [4] as well as other methods [11, 12]. We also distinguish between fully automatic [10, 15, 4, 11], and semi-automatic [14] vessel segmentation algorithms where the latter typically need some user supplied seed points (points which belong to the vessel class with a high probability). Our segmentation algorithm follows the two step approach described above. In a first feature extraction step, a multidimensional pixel feature space is built. The vessels are then segmented in an unsupervised manner, starting from an over-segmentation with practically no false negatives which is thinned out stepwise to produce a final result. The results of each iteration step are stored for potential interactive access. The obtained segmentation typically exhibits many false positives. Based on the observation that vessels exhibit bendings and bifurcations we then select true vessels using automatically detected corners as seed points. If the user is not satisfied with the automatic result he or she may then manually refine it using the results of all iteration steps.

2. The pixel feature space

The main feature extraction goal is to increase the separability between the vessel and the background pixel classes with separability defined by the J_1 separability criterion [8, pp. 466]. Thus we try to obtain a feature space with hyperellipsoidal shaped clusters which is well suited for a successful unsupervised segmentation by a clustering algorithm [2]. We enhance vessel information in several ways mainly based on the observation that vessels are tubular structures of a certain size which appear darker than their immediate surroundings. Each time we obtain a vessel map. For each pixel we build a feature vector by ordering its scalar features in each vessel map into a vector. Within each vessel map we seek to increase the separability between the background and vessel pixel classes by achieving a homogeneous gray-level representation (i.e. small intra-class variance) for both background and vessels and/or a large contrast (i.e. large inter-class variance). Our strategy is then to combine the results of several different enhancement methods in the hope that together they constitute a highly separable representation of vessels and background.

2.1. Top-hat filtering

The Top-hat filter is defined as the difference between the original image and its morphologically closed version [6]. Using as structuring element a disk with diameter slightly larger than the vessel diameter ideally yields a vessel-only image. With respect to the separability, the benefit of the top-hat filter is twofold: first, it tends to equalize the background to a constant value, resulting in a very low intra-background class variance. Simultaneously, it also reduces the intra-vessel class variance. The reason for this is the superposition of vessel and background in X-ray projection imaging. Assuming that the angiograms underwent a logarithmic point transform, this superposition is additive. The intensity representation of a vessel with a given size thus depends not only on the vessel absorption itself, but varies also with background absorption. Background equalization removes this influence on the vessel representation, so that only the variability of the vessel thickness remains. A result obtained after reversing the logarithm by an exponential is shown in Fig. 1b.

2.2. Hessian based vessel enhancement

The Hessian matrix describes the second order structure of gray-level variations around each point of the image $f(x, y)$ [7]. By eigenanalysis of the Hessian matrix dark elongated objects (i.e. vessels) may be found at the positions where the first eigenvalue is positive and prominent. To increase the separability we try to reduce the vessel class variance by enhancing the vessels comparably irrespective of their size. Thus we decompose the Top-hat result on a Gaussian pyramid

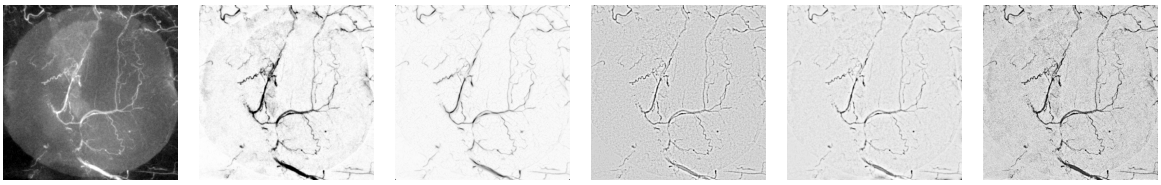

(a) (b) (c) (d) (e) (f)

Figure 1. Vessel enhancement. Original image (a), Top-hat (b), Hessian based (c), homomorphic filter (d), Laplacian pyramid based (e), non-linear filter (f)

with three levels and compute the largest Hessian eigenvalue at different scales. The derivative operators should be chosen such that they respond to the smallest theoretically observable vessel. To avoid noise boosting the pyramid levels are low-pass filtered before computing the Hessian matrix. We then interpolate the results obtained at each scale back to the original resolution and combine them pixel-wise by the maximum rule. A result is shown in Fig. 1c.

2.3. Homomorphic filter

Homomorphic filtering is a general procedure for analyzing the result of a multiplication between two different signals [13]. As a vessel enhancement method it is motivated by the image acquisition model. In a first step the logarithm of the input is calculated, thus reversing the exponential. After exponentiation the two underlying signals are additively combined. To eliminate the background and enhance the vessels we apply a shift-invariant high-pass filter. The high frequency components are obtained after subtracting from the original sum its low-pass filtration result. To increase the vessel contrast an amplification of the high-pass channel by a factor larger than one follows. In a last step, the exponential of the high-pass filtration result is computed. A result is shown in Fig. 1d.

2.4. Vessel enhancement using Laplace pyramid decomposition

The large vessel class variance is mainly generated by the fact that the vessel contrast increases with the size. Thus, we decompose the Top-hat result on a Laplacian pyramid [3] with four levels (plus a low-pass level) to gain individual access to each vessel category (from small to large) and to the background. Then at reconstruction we ignore the low-pass background information and amplify the subbands containing vessel information with positive weights chosen according to a Gauss-like function of the subband index. We justify this procedure by the observation that to reduce the variance, the small vessels need to be stronger amplified than the mid vessels which in turn need a stronger amplification than the large vessels, while at the same time the high-pass subband contains primarily noise which we do not want to increase. A result is shown in Fig. 1e.

2.5. Reducing the vessel class variance by nonlinear filtering

Yet another way of reducing the vessel class variance is by filtering the image such that large structures are stronger suppressed than smaller ones. The vessel map is then computed by taking the square root of the magnitude spectrum of the Top-hat result. We justify the use of the square root rather than a typical high-pass characteristic by observing that after Top-hat filtering we have practically only vessels left. Thus we do not want to completely eliminate the low frequency structures (i.e. large vessels) but only to attenuate them thus reducing the vessel class variance. A result is shown in Fig. 1f.

3. Binary vessel-background pixel classification

For vessel segmentation, we use a clustering algorithm with better classification performance in comparison to other standard techniques [2]. It iteratively improves a clustering performance measure computed on a fuzzy set decomposition, starting from an initial partition. To allow easy and comfortable interactive processing this partition is an over-segmentation. Furthermore, since thus practically every vessel is visible at a certain stage during the iterations, this permits to achieve better results at the end of the processing chain. The use of a clustering algorithm is justified by the desire to keep the generality of the method and by the fact that we do not have access to an expert-labeled training set. After the iteration stops, we automatically choose the desired vessel segments by corner analysis. In case the user is not quite satisfied with the automatically provided result, he or she may then manually refine the segmentation.

3.1. Fuzzy clustering

The clustering algorithm is initialized with a vessel over-segmentation result computed by thresholding the Top-hat vessel map. Empirically, the vessel covered area is always less than 50% of the image area, thus we choose the 50th percentile as threshold. A result is shown in Fig. 2a.

The fuzzy class memberships are computed by a function (i.e. affinity) which measures how closely related the investigated vector is to a certain class. Let $\vec{x}$ be one from a set of N feature vectors, and ω_i be one from a set of M classes. The affinity of $\vec{x}$ to ω_i is defined as: $r(\vec{x},\omega_i) = 1 - \frac{1}{N}\sum_{\vec{y}\in\omega_i} h^\beta(\parallel \vec{x}-\vec{y} \parallel)$ with $h^\beta : [0,\infty) \rightarrow [0,1]$ and: $h^\beta(\nu) = \begin{cases} \frac{\nu^2}{\beta} & \text{if } \nu \leq \sqrt{\beta} \\ 1 & \text{if } \nu > \sqrt{\beta} \end{cases}$ Then the class belonging coefficient for $\vec{x}$ and ω_i is: $u_i(\vec{x}) = P_i \frac{r(\vec{x},\omega_i)}{r(\vec{x},U)}$, with P_i the prior on ω_i. The parameter β is actually a bound on the cluster/class spread. Feature vectors further apart than $\sqrt{\beta}$ are ignored in the affinity computation. Choosing β such that $\max \parallel \vec{x} - \vec{y} \parallel = \sqrt{\beta_m}$ for $\vec{x},\vec{y} \in U$ permits the consideration of all feature space points. Then, representing each class by its mean vector alone, the fuzzy class membership coefficients will be: $u_i(\vec{x}) = \frac{\beta - \|\vec{x}-\mu_i\|^2}{\beta M - \sum_{j=1}^{M}\|\vec{x}-\mu_j\|^2}$ and $\sum_i^M u_i(\vec{x}) = 1$. Although heuristic methods for determining β are available in [2], for vessel segmentation we propose on an empirical basis choosing β such that $\sqrt{\beta} = 0.8\sqrt{\beta_m}$. For vectors beyond the allowed spread $u_i = 0$. To measure the quality of a certain fuzzy partition (i.e. the amount of incertitude (fuzziness) present), the following function is used: $\Psi = \frac{1}{N(M-1)} \sum_{i=1}^{M-1} \sum_{j=i+1}^{M} \sum_{\vec{x}\in U} (u_i(\vec{x}) - u_j(\vec{x}))^2$ with $\Psi \in [0,1]$ and $\Psi = 0$ indicating the highest possible degree of fuzziness.

Then during an iteration a vector will change its class only if it leads to an increase in the quality of the fuzzy partition. The iterations stop when Ψ can not be increased anymore. To successfully meet the challenge of a correct vessel segmentation in micro-angiograms (i.e. strongly unbalanced class sizes and inner-class variances) we have extended the fuzzy clustering algorithm to use an additional statistically motivated stopping criterion based on the same separability measure which guided also the feature extraction process. Then the algorithm will stop as soon as the separability measured on the current vessel class fuzzy coefficients set decreases. As ground truth the segmentation result obtained at the end of the previous iteration is used. A result is shown in Fig. 2b.

3.2. Seed points based vessel selection

The segmentation obtained by fuzzy clustering typically exhibits many false positives. We use a seed points based selection mechanism to determine the real vessels. As a typical vessel tree shows multiply oriented regions (i.e. bendings, bifurcations, etc.) while the background does not,

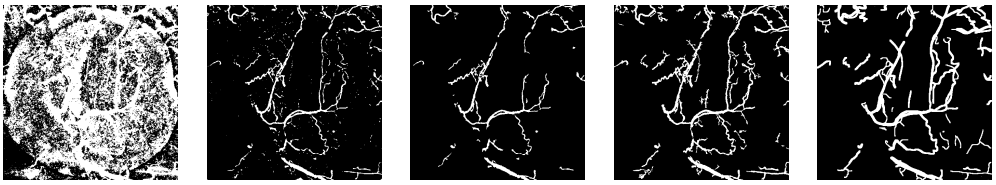

(a) (b) (c) (d) (e)

Figure 2. Segmentation results. Initial partition (a), automatic result before (b) and after (c) corner selection, user supported result (d), fully manual segmentation (e)

we use corner points as seeds. The corners are detected by thresholding the lower eigenvalue image of the tensor describing the orientation in a certain neighborhood [1]. All segmented vessel points connected to a corner by an eight points neighborhood are selected in the final segmentation. A result is shown in Fig. 2c. This corner based vessel selection mechanism will clearly fail for straight vessels and it will also respond to small dark patches (i.e. when both structure tensor eigenvalues are large). Thus, if the user is not satisfied with the automatic result he may then refine it by deselecting false vessels with "negative" seed points and/or by browsing through the segmentation results (which were saved at the end of each iteration step and which show less and less false positives) and adding vessel structures to the segmentation from that iteration result which he considers appropriate by "positive" seed points. A result is shown in Fig. 2d.

4. Results

As of present we have used ten micro-angiograms (512x512 pixels large) to evaluate our algorithm both with respect to the quality of the feature extraction process and the segmentation results. As reference we have used fully manual segmentation results performed by the first author. The quality of the feature space was measured by the J_1 separability criterion. For the original image the mean separability was 0.2050, for the Top-hat result (the most separable single vessel map) 0.4895 and for the multidimensional feature space 0.6527. Vessel enhancement results are shown in Fig. 1. The segmentation performance is evaluated by means of the mean percentages of correct classifications and false positives. The percentage of correctly classified vessel pixels before and after corner based selection was 76.9725% and 62.6390% and the percentage of falsely classified background pixels was 6.0375% and 2.1658% respectively. With user supported vessel selection, 84.6881% of the vessel pixels were correctly classified and 4.0534% of the background pixels were falsely classified. Segmentation results for the micro-angiogram of Fig. 1a are shown in Fig. 2.

We are finally interested in measuring the vessel area and length [9]. After segmentation, the vessel area can be computed as the sum of all vessel pixels. To compute the vessel length, a skeletonization procedure should first be applied to the segmentation result followed by a summation.

5. Discussion and conclusions

We distinguish between critical false positives (i.e. vessel chunks not segmented) and less-critical false positives which appear at the margins of true vessels, some of which are even due to a non-perfect ground truth. User supported vessel selection increases the number of the less-critical false positives as now more vessels are segmented. These could influence the area measurements but as we are interested to compare the angiogenesis in two (or more) cases rather than to precisely measure vessel surface in each case, consistent errors which affect both measurements in the same

way are less severe. Clearly, the vessel length measurements could only marginally be influenced by these false positives. We are currently investigating the precise role played by false positives at vessel edges in our analysis.

We have presented a novel framework for imaging and analysis of micro-vessels in skin transplants in laboratory environments for drug testing. For imaging, a specific micro-angiography technique was described, followed by an analysis tool. Central to the analysis part is a micro-vessel segmentation algorithm, the results of which are used for vessel area and vessel length measurements in skin transplant micro-angiograms. As we do not have access to a training set but also to ensure the adaptability and thus the generality required for a successful segmentation of vessels, each micro-angiogram is individually analyzed. In a first step a multidimensional pixel feature space is build by gathering the results of several vessel enhancement methods so that together they constitute a separable description of vessels and background. The segmentation algorithm then returns (after several iterations) image structures likely to be vessels. As a key vessel feature, we use the fact that they typically exhibit branchings, i.e. local structures with so-called corners, which may be detected by an inertia matrix approach. The detected branching points (or corners) are then used as seed points. A structure which appears in the final segmentation result is identified as vessel only if it is connected to such a seed point. Experience shows that the result may still contain some false positives and false negatives. Since our system's field of application is an experimental laboratory setting for drug evaluation rather than clinical routine, time-constraints are of less concern and a certain degree of interaction is feasible. Thus the experimenter is allowed to manually refine the segmentation by browsing through the results of the iteration steps, and select or deselect vessel structures by placing "positive" and "negative" seed points respectively.

References

[1] T. Aach, I. Stuke et al. Estimation of multiple local orientations in image signals. In *Proceedings of ICASSP*, pp.: 553–556, 2004.

[2] E. Backer, A. K. Jain. A clustering performance measure based on fuzzy set decomposition. *IEEE TPAMI*, 3(1):66–75, 1981.

[3] P. J. Burt, E. H. Adelson. The laplacian pyrmaid as compact image code. *IEEE T Comm.*, 31(4):532–540, 1983.

[4] Z. Chen, S. Molloi et al. Multiresolution vessel tracking in angiographic images using valley courses. *Opt. Eng.*, 42:1673–1682, 2003.

[5] A. P. Condurache, T. Aach. Vessel segmentation in angiograms using hysteresis thresholding. In *Proceedings of MVA*, 2005. to appear.

[6] E. R. Dougherty. *Mathematical morphology in image processing*. Marcel Dekker, 1992.

[7] A. F. Frangi, W. J. Niessen et al. Multiscale vessel enhancement filtering. *LNCS*, 1496:130–137, 1998.

[8] K. Fukunaga. *Introduction to statistical pattern recognition*. Academic Press, 1990.

[9] S. Grzybowski, B. Bucsky et al. A microangiography technique to quantify fasciocutaneous blood vessels in small laboratory animals. *Langenbeck's Archive of Surgery*, 389(10), 2004.

[10] A. Hoover, V. Kouznetzova et al. Locating blood vessels in retinal images by picewise threshold probing of a matched filter response. *IEEE TMI*, 19(3):203–210, 2000.

[11] X. Jiang, D. Mojon. Adaptive local thresholding by verification based multithreshold probing with application to vessel detection in retinal images. *IEEE TPAMI*, 25(1):131–137, 2003.

[12] C. Kerbas, F. K. H. Quek. A review of vessel extraction techniques and algorithms. *http://vislab.cs.vt.edu/review/extraction.html*, 2002.

[13] A. V. Oppenheim, R. W. Schafer et al. Nonlinear filtering of multiplied and convolved signals. *Proceedings of the IEEE*, 56(8):1264–1291, 1968.

[14] D. Selle, B. Preim et al. Analysis of vasculature for liver surgical planning. *IEEE TMI*, 21(11):1344–1357, 2002.

[15] J. Staal, M. D. Abramoff et al. Ridge-based vessel segmentation in color images of the retina. *IEEE TMI*, 23(4):501–509, 2004.